ORIGINAL RESEARCH

Multiple Approaches to Diffusion Magnetic Resonance Imaging in Hereditary Cerebral Amyloid Angiopathy Mutation Carriers

Tijn M. Schouten, MSc; Frank de Vos, MSc; Sanneke van Rooden, PhD; Mark J. R. J. Bouts, PhD; Anna M. van Opstal, PhD; Rogier A. Feis, MSc; Gisela M. Terwindt, PhD; Marieke J. H. Wermer, PhD; Mark A. van Buchem, PhD; Steven M. Greenberg, PhD; Mark de Rooij, PhD; Serge A. R. B. Rombouts, PhD; Jeroen van der Grond, PhD

***Background*—**Cerebral amyloid angiopathy (CAA) is a major cause of lobar intracerebral hemorrhage in elderly adults; however, presymptomatic diagnosis of CAA is difficult. Hereditary cerebral hemorrhage with amyloidosis–Dutch type (HCHWA-D) is a rare autosomal-dominant disease that leads to pathology similar to sporadic CAA. Presymptomatic HCHWA-D mutation carriers provide a unique opportunity to study CAA-related changes before any symptoms have occurred. In this study we investigated early CAA-related alterations in the white matter.

***Methods and Results*—**We investigated diffusion magnetic resonance imaging (dMRI) data for 15 symptomatic and 11 presymptomatic HCHWA-D mutation carriers and 30 noncarrier control participants using 4 different approaches. We looked at (1) the relation between age and global dMRI measures for mutation carriers versus controls, (2) voxel-wise dMRI, (3) independent component-clustered dMRI measures, and (4) structural connectomics between presymptomatic or symptomatic carriers and controls. Fractional anisotropy decreased, and mean diffusivity and peak width of the skeletonized mean diffusivity increased significantly over age for mutation carriers compared with controls. In addition, voxel-wise and independent component-wise fractional anisotropy, and mean diffusivity, and structural connectomics were significantly different between HCHWA-D patients and control participants, mainly in the periventricular frontal and occipital regions and in the occipital lobe. We found no significant differences between presymptomatic carriers and control participants.

***Conclusions*—**The dMRI technique is sensitive in detecting alterations in symptomatic HCHWA-d carriers but did not show alterations in presymptomatic carriers. This result indicates that dMRI may be less suitable for identifying early white matter changes in CAA. **(*J Am Heart Assoc*. 2019;8:e011288. DOI: 10.1161/JAHA.118.011288.)**

Key Words: cerebral amyloid angiopathy • diffusion magnetic resonance imaging • hemorrhage • hereditary cerebral amyloid angiopathy • magnetic resonance imaging

Sporadic cerebral amyloid angiopathy (CAA) is a highly prevalent disease in elderly adults that is characterized by deposition of amyloid-β peptides in the media and adventitia of small leptomeningeal and cortical vessels, causing hemorrhagic lesions.[1] Although CAA is a major cause of lobar intracerebral hemorrhage,[2,3] reliable in vivo diagnosis of sporadic CAA is difficult, especially in the early stage of the disease. Still, from a therapeutic viewpoint, the early—presymptomatic—phase of the disease is of particular interest. In contrast with the symptomatic phase of the disease, which is characterized by the occurrence of hemorrhagic lesions, no reliable biomarkers for disease severity or progression have been established for the presymptomatic phase. Because accumulation of amyloid-β in the vessel walls and loss of vascular smooth muscle cells are present before symptoms, it has been suggested that in sporadic CAA, ischemia-[4–7] or hemorrhage-related[7–9] alterations in the white matter may already be present in the early, presymptomatic stage of the disease. Diffusion tensor imaging (DTI) is able to detect altered white matter in probable CAA.[10–15]

Hereditary cerebral hemorrhage with amyloidosis–Dutch type (HCHWA-D) is an autosomal-dominant disease and

From the Departments of Radiology (T.M.S., F.d.V., S.v.R., M.J.R.J.B., A.M.v.O., R.A.F., M.A.v.B., S.A.R.B.R., J.v.d.G.) and Neurology (G.M.T., M.J.H.W.), Leiden University Medical Center, Leiden, The Netherlands; Leiden Institute for Brain and Cognition (T.M.S., F.d.V., S.v.R., M.J.R.J.B., R.A.F., M.d.R., S.A.R.B.R.) and Institute of Psychology (T.M.S., F.d.V., M.J.R.J.B., M.d.R., S.A.R.B.R.), Leiden University, Leiden, the Netherlands; Department of Neurology, Massachusetts General Hospital, Boston, MA (S.M.G.).

Correspondence to: Tijn M. Schouten, MSc, Department of Radiology, Leiden University Medical Center; Leiden Institute for Brain and Cognition; and Institute of Psychology, Leiden University, Leiden, the Netherlands. E-mail: t.m.schouten@fsw.leidenuniv.nl

Received November 8, 2018; accepted December 13, 2018.

© 2019 The Authors. Published on behalf of the American Heart Association, Inc., by Wiley. This is an open access article under the terms of the Creative Commons Attribution-NonCommercial License, which permits use, distribution and reproduction in any medium, provided the original work is properly cited and is not used for commercial purposes.

Clinical Perspective

What Is New?

- This study is the first to extensively investigate diffusion magnetic resonance imaging in a presymptomatic sample of hereditary cerebral hemorrhage with amyloidosis–Dutch type mutation carriers who will develop symptoms similar to cerebral amyloid angiopathy.
- Diffusion magnetic resonance imaging shows widespread white matter alterations in symptomatic mutation carriers.
- Alterations in diffusion magnetic resonance imaging measurements could not yet be detected in presymptomatic mutation carriers.

What Are the Clinical Implications?

- Diffusion magnetic resonance imaging may be less suitable to detect early changes in cerebral amyloid angiopathy.

occurs predominantly in the Netherlands.[16] The mutation leads to extensive amyloid-β deposition in the meningocortical arterioles. The underlying pathology of these amyloid deposits is similar to that in sporadic CAA with minimal or no neurofibrillary pathology.[17–19] Therefore, HCHWA-D may serve as a hereditary CAA model for studying early, presymptomatic, cerebral changes. In the present study we aimed to investigate the potential of diffusion tensor magnetic resonance imaging (MRI) to determine alterations in the white matter of presymptomatic HCHWA-D mutation carriers and symptomatic HCHWA-D patients compared with control participants.

Methods

The data that support the findings of this study are available from the corresponding author on reasonable request.

To analyze the diffusion MRI (dMRI) data, we applied 4 approaches. First, we explored the differences in the aging effect of DTI parameters between mutation carriers and controls.[20] Second, to get a more fine-grained image of differences between presymptomatic carriers and controls and symptomatic carriers and controls, we investigated voxel-wise DTI measures. Third, to increase power, we clustered the voxel-wise diffusion tensor measures into independent components (ICs). Finally, we investigated the structural connectivity between cortical brain areas using structural connectomics.

Participants

Participants were selected via the HCHWA-D patient association in Katwijk (the Netherlands) and the outpatient clinic of the Department of Neurology of the Leiden University Medical Center based on DNA analysis for confirmation of a point mutation in the APP gene (amyloid precursor protein; p.Glu693Gln mutation). Twenty-six DNA-proven HCHWA-D mutation carriers were included in the present study, of which 15 were symptomatic and 11 were presymptomatic. Participants were considered symptomatic if they had reported symptoms associated with HCHWA-D to a general practitioner. Thirty control participants were recruited from individuals at risk for HCHWA-D, for whom one parent had HCHWA-D, and from participant spouses, family members, or friends. All controls were stroke-free and tested genetically negative for HCHWA-D. Investigators remained completely blinded concerning the genetic status of participants during recruitment, MRI, and neurological and psychological exams. At the time of the study, a third of the potential mutation carriers were not aware of their genetic status. Table shows the demographic overview of the study sample. The ethics committee of our institution approved the study, and written informed consent was obtained from all participants.

MRI Acquisition and Image Processing

Each participant was scanned at the Leiden University Medical Center on a Philips Achieva 3T MRI scanner (Philips Medical Systems) using an 8-channel head coil. Anatomical 3-dimensional T1-weighted images were acquired with repetition time of 9 ms, echo time of 4.6 ms, flip angle of 8°, and field of view of $224\times177\times168$ mm^3. Diffusion images were acquired along 32 noncollinear directions with a b-value of 1000 s/mm^2, along with a b=0 image with repetition time of 9033 ms, echo time of 56 ms, flip angle of 90°, 64 axial slices, voxel size of $1.96\times2.00\times2.00$ mm^3, matrix size of $112\times110\times64$, and field of view of $220\times220\times128$ mm^3.

The dMRI data were preprocessed using the FMRIB software library (v5.0.8)[21,22] and MATLAB (R2016b). This consisted of brain extraction, motion correction, and eddy current correction. The FMRIB software library program *dtifit* was used to calculate individual fractional anisotropy (FA) and mean diffusivity (MD). FA images were subsequently nonlinearly registered to the FMRIB58 FA template for individual registration to Montreal Neurological Institute (MNI) space.

Group differences in voxel-wise DTI measures were investigated with tract-based spatial statistics (TBSS) using default settings.[23] This procedure projects the center of each subject's white matter tracts onto a mean white matter tract. This allows for voxel-wise statistical analyses of FA and MD. The global FA or MD was the average FA or MD value of all voxels that were projected onto the TBSS skeleton. As an additional global measure we investigated the peak width of the skeletonized MD (PSMD),[24] which has been specifically validated as a marker for small vessel disease.

Table. Baseline Characteristics of Presymptomatic and Symptomatic Mutation Carriers Versus Controls

	Controls (n=30)	Presymptomatic Carriers (n=11)	Symptomatic Carriers (n=15)
Age, y	44.7 (13.7; 34–56)	33.2 (11.9; 22–46)*	55.1 (5.2; 51–60)*
Sex (male/female), n	11/19	3/8	7/8
Systolic blood pressure	129.9 (27.2; 106–142)	124.6 (14.9; 110–133)	144.2 (19.8; 129–168)
Diastolic blood pressure	81.9 (12.5; 72–87)	79.8 (9.6; 73–87)	89.1 (10.4; 78–96)
Mean arterial pressure	97.9 (16.5; 84–108)	94.7 (9.6; 88–102)	107.5 (12.4; 95–117)
Pulse pressure	48.0 (18.9; 34–58)	44.7 (13.9; 33–50)	55.1 (14.7; 43–69)
Hypertension, %	20	0	40
Hyperlipidemia, %	7	0	33*
Diabetes mellitus, %	0	9	7
Cardiovascular disease, %	0	0	7

Data are shown as mean (SD; interquartile range), except as noted.
*Indicates significant difference with controls.

To reduce the dimensionality of the data, we clustered the voxel-wise measures with IC analysis. This procedure identifies clusters of voxels that show similar patterns across participants and characterizes each person with a weight for each component. Specifically, we used Multivariate Exploratory Linear Optimized Decomposition into Independent Components (MELODIC)[25] to decompose each of the skeletonized FA and MD maps into 10 ICs (ie, the *IC number*). This resulted in 10 spatial IC weight maps and, for each participant, a mixing weight per component. The differences in mixing weights could then be compared across groups. This procedure increases power by reducing the dimensionality from >100 000 voxel values to just 10 mixing weights.

The structural connectomics were constructed with probabilistic tractography between Harvard–Oxford cortical and subcortical atlas regions.[26,27] For this purpose, the 48 cortical regions of the Harvard–Oxford cortical atlas were split into left and right hemisphere regions, resulting in 96 cortical regions. These were combined with 14 of the 15 regions from the Harvard–Oxford subcortical atlas, excluding the brain stem. These 110 probabilistic gray matter (GM) regions were given thresholds of 25% probability and voxel-wise assigned to the region with the highest probability.

Probabilistic tractography was conducted using anatomically constrained tractography[28] with spherical-deconvolution informed filtering of tractograms, or SIFT,[29,30] as implemented in *mrtrix* (v3.0_RC3-1).[31] For anatomically constrained tractography, the T1-weighted image was aligned to the b=0 image using rigid-body registration. Partial volume estimates of white matter, cerebrospinal fluid (CSF), and cortical GM were calculated using the FMRIB automated segmentation tool (FAST),[32] and subcortical cortical GM estimates—excluding the brain stem—were calculated with the FMRIB integrated registration and segmentation tool.[33] Fiber orientation distributions were estimated using constrained spherical deconvolution with recursive calibration for fiber response function estimation[34] and maximum spherical harmonic order of 6. The second-order integration over fiber orientation distributions algorithm[35] was used to generate 5 million streamlines (seeding: GM–white matter interface; step size=1.0 mm; maximum curvature=45° per step; length: 2–200 mm; and fiber orientation distribution threshold=0.0625), which were reduced to 50 000 streamlines using SIFT. Structural connectivity graphs were constructed by summing the regional streamlines that were assigned to the closest Harvard–Oxford GM region within a 2-mm radius of each streamline end point.[36] This resulted in a 110×110 matrix of SIFT-filtered streamline counts between the regions. Subsequently, we used the MATLAB implementation of the brain connectivity toolbox (http://www.brain-connectivity-toolbox.net) to calculate the strength, degree, clustering, and betweenness centrality[37] of each node in the connectivity graph, resulting in 1 value per person per region and 110 values in total per person. In addition, we characterized each participant's graph with transitivity and global efficiency,[13] resulting in a single value per participant.

To correct the data for CSF partial-volume effects, we calculated the proportion of CSF of the total intracranial volume using the segmentations from FAST.

Statistical Analysis

For demographics, the Mann–Whitney *U* test was used to assess differences in age between groups; univariate general linear modeling analysis was used to assess differences in blood pressure measurements between groups, adjusted for age and sex; and χ^2 tests were used to assess differences in sex and percentage cardiovascular risk factors between groups.

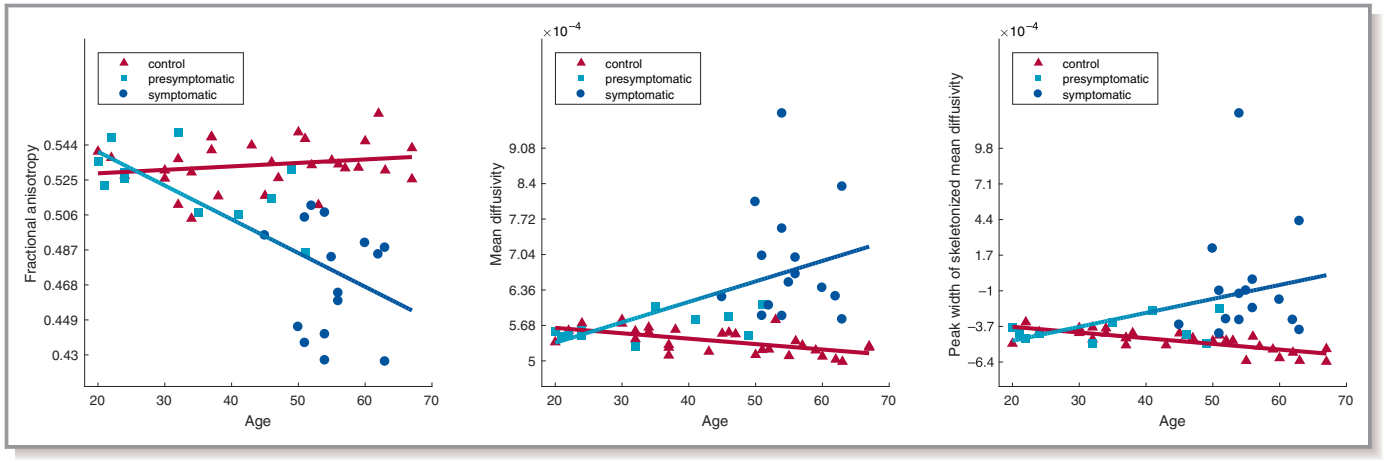

Figure 1. Scatterplot of the relation between age and fractional anisotropy (left), mean diffusivity (middle), and peak width of skeletonized mean diffusivity (right) for presymptomatic mutation carriers, symptomatic patients, and control participants. The measures are adjusted for sex and proportional cerebrospinal fluid. The blue line indicates the trend for mutation carriers (symptomatic and presymptomatic combined), and the red line indicates the trend for controls.

To analyze the DTI data, we first explored the effect of gene presence on the decline in global, whole-brain FA, MD, and PSMD over age, namely, the interaction between age and gene presence. In addition, we explored the presence of a quadratic effect of age on the diffusion measures. To do this, we fitted 3 regression models for each of the 3 DTI measures. As covariates, we included sex and proportional CSF. The reduced model included age and gene presence. The linear age×gene interaction model also included age×gene interaction. The quadratic age×gene interaction model also included age^2 and age^2×gene. We used partial *F* tests for testing the increase in explained variance of the linear age×gene interaction model compared with the reduced model and for the quadratic age×gene interaction model compared with the linear age×gene interaction model. To determine significance and to correct for multiple comparisons across all 6 tests (3 measures and 2 comparisons), we used permutation testing with 5000 permutations.

Second, we used a general linear model with age, proportional CSF, and sex as covariates to test the differences between controls and presymptomatic carriers and between controls and symptomatic patients. For the voxel-wise analyses, threshold free cluster enhancement was performed to use spatial neighborhood information.[38] The same general linear model was used for the IC analysis clustered mixing matrices and for the graph measures.

To correct for multiple comparisons, we used the *permutation analysis of linear models* tool[39] with 500 permutations and tail approximation for accelerated permutation inference[40] for the voxel-wise TBSS and 5000 permutations without tail approximation for the other approaches. For each of the latter 3 approaches, the reported *P* values were familywise error corrected across all tests, contrasts, and modalities within each of 3 approaches: (1) voxel-wise TBSS, (2) IC analysis×clustered TBSS measures, and (3) probabilistic tractography–based graph measures.

Results

Global Diffusion Measures Over Age

The age×gene interaction model explained significantly more variance than the reduced model without gene interaction for FA, MD, and PSMD at F(1, 50)=23.51, 14.73, and 9.68, respectively, with corresponding permutation familywise error–corrected *P* values: *P*<0.001, *P*=0.001, *P*=0.011 (see Figure 1). Adding quadratic terms did not improve the models for any of the measures, F(2, 48)=0.13, 0.19, and 0.27, respectively; all familywise error–corrected *P* values were not significant.

TBSS Analysis

The tract-based spatial statistics results for FA and MD comparing HCHWA-D patients with control participants are shown in Figure 2. We found lower FA values in symptomatic HCHWA-D patients compared with control participants, especially in the parietal and occipital lobes. In symptomatic HCHWA-D patients, MD was increased in the white matter, especially in the periventricular frontal and occipital regions and in the centrum semiovale. No differences between presymptomatic HCHWA-D mutation carriers and control participants were found.

IC Analysis

Symptomatic carriers and controls differed significantly on 4 IC mixing weights for FA (see Figure 3, left). The bars

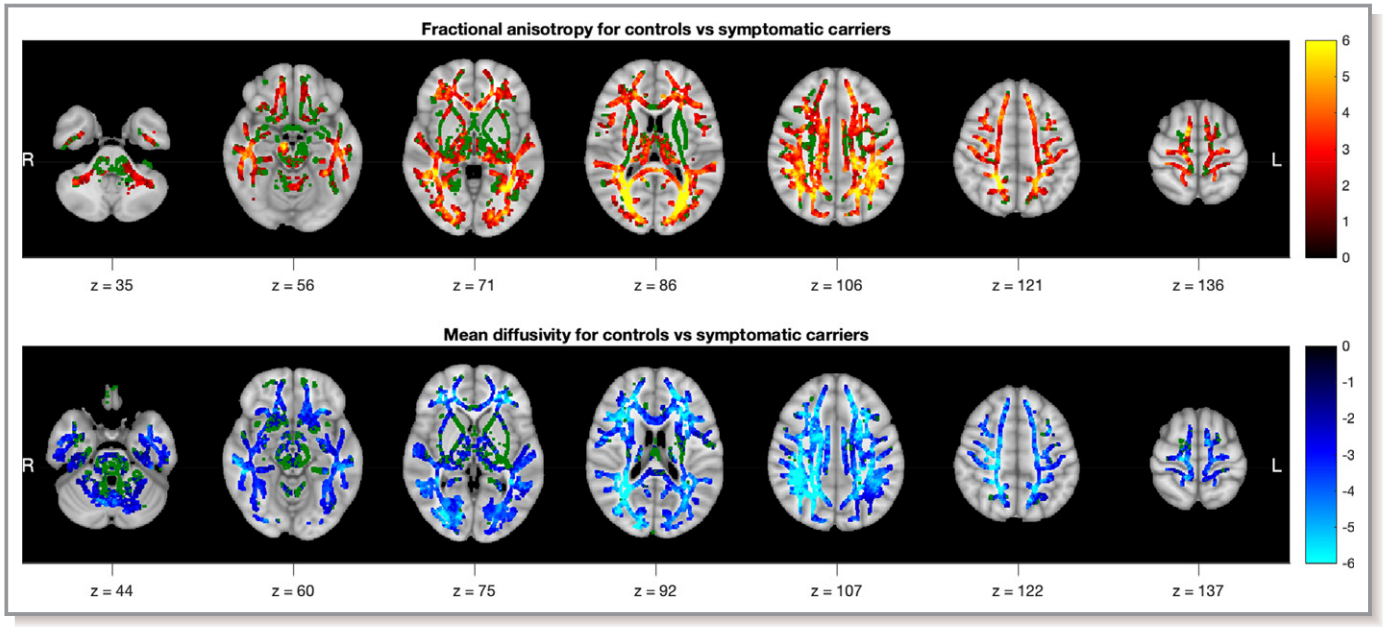

Figure 2. Control vs symptomatic carriers' *t* statistics, $P<0.05$ familywise error corrected across modalities, contrasts, and voxels. Tract-based spatial statistics skeleton background is plotted in green. The tract-based spatial statistics skeleton was dilated with 1 voxel for visualization purposes.

represent the average mixing weight of each component for each individual group, corrected for age, sex, and proportional CSF. This analysis shows that, for both FA values, the components that differed significantly had high component importance mainly in the occipital and parietal lobes. For MD, 3 ICs were identified that differed significantly between symptomatic carriers and controls (Figure 3, right). Overall, high component importance was located mainly in periventricular frontal and occipital regions and the occipital lobe. No significant differences between presymptomatic mutation carriers and control participants were found.

Structural Connectomics Analyses

Figure 4 shows the results of the structural connectomics analyses between brain areas. This analysis reveals structural connectivity of cortical GM structures rather than intrinsic white matter tract information. Our analyses showed that the degree of structural connectivity is lower in 7 cortical regions for symptomatic carriers compared with controls (see Figure 4, left). In addition, in 1 of these regions, the left cuneal cortex, the clustering was higher for symptomatic carriers compared with controls (see Figure 4, middle). Furthermore, the betweenness centrality was higher for symptomatic carriers compared with controls in 2 regions (see Figure 4, right). We found no differences in strength, transitivity, or global efficiency. None of the measures showed significant differences between presymptomatic carriers and controls.

Discussion

Our data show that differences in DTI and DTI-related connectivity parameters between HCHWA-D patients and control participants are mainly located in the periventricular frontal and occipital regions and in the occipital lobe. We found no significant differences in any of these parameters between presymptomatic HCHWA-D mutation carriers and control participants.

In our first analysis, we found a greater decrease in global FA and a greater increase in global MD and PSMD over age for mutation carriers than for controls. White matter integrity appears largely unaffected in the presymptomatic phase and then deteriorates in a later stage, when mutation carriers become symptomatic. PSMD has been validated as a marker for small vessel disease,[24] but it was remarkably similar to global MD in our findings.

All our dMRI analyses were sensitive to differences between controls and symptomatic carriers, whereas no significant differences were found between presymptomatic mutation carriers and control participants. The symptomatic carriers had reduced FA and increased MD in widespread areas of the brain, covering almost the entire white matter skeleton. Reduced FA and increased MD is associated with altered white matter. The effects were most pronounced in the periventricular frontal and occipital regions and in the occipital lobe of the brain. The same trend arose from IC analysis–clustered diffusion tensor measures. ICs that contributed strongly toward the posterior regions of white matter

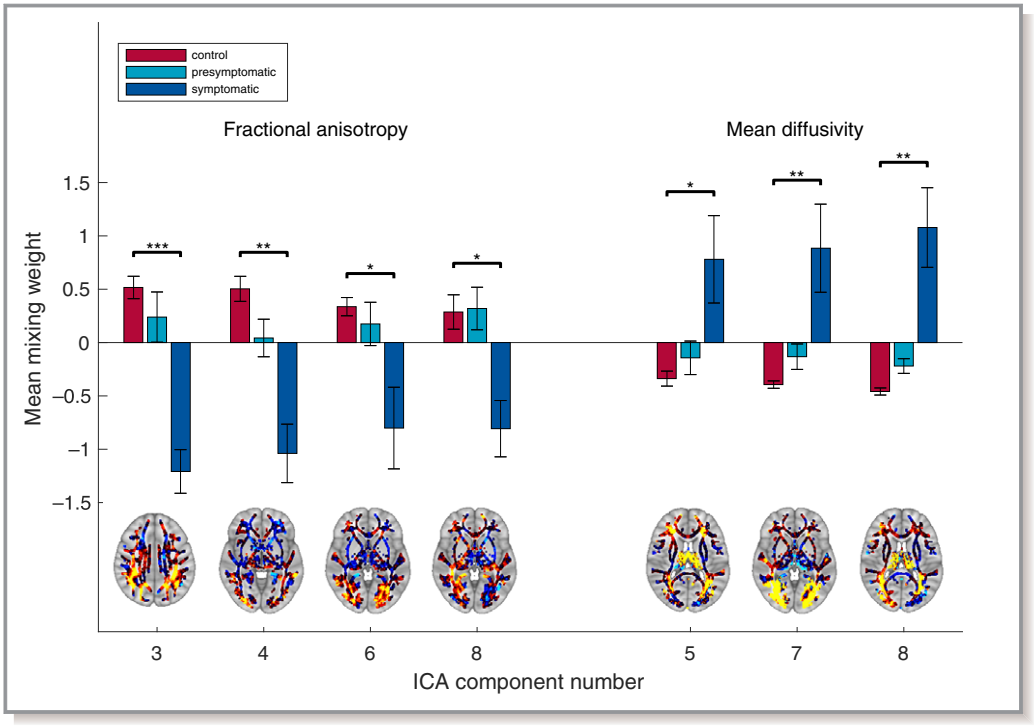

Figure 3. Independent component mixing weights for fractional anisotropy and mean diffusivity, with *z* scores for display purposes. Means adjusted for age, sex, and proportional cerebrospinal fluid. The tract-based spatial statistics skeleton was dilated with 1 voxel for visualization purposes. Red-yellow indicates positive values of the weight maps (yellow is higher), whereas blue-cyan indicates negative values of the weight maps (cyan is more negative). **P*<0.05, ***P*<0.01, ****P*<0.001. (Familywise error corrected for components, measures, and contrasts.) ICA indicates independent component analysis.

showed a significant difference between symptomatic carriers and controls. This finding is also indicative of altered white matter, specifically in the posterior regions of the brain. The finding that the occipital region is most severely affected is in line with previous findings that the occipital lobe is a predilection site of CAA.[41,42] Structural connectomics revealed a lower connection degree for symptomatic carriers compared with controls in several cortical, mainly posterior, regions, indicating fewer connections between these regions and the rest of the brain. Furthermore, clustering was higher in one of these regions. This finding is to be expected because this region has fewer neighbors, so it is more likely that these neighbors would be connected to each other. Furthermore, a decrease in degree and an increase in clustering is typical for a hierarchical network, and the structural connectivity graph has been found to show these characteristics.[43] Furthermore, betweenness centrality was higher in 2 regions for symptomatic carriers compared with controls. It is likely that because of the decrease in connections in the symptomatic patients, many of the shortest paths between nodes must pass through relatively unaffected regions, resulting in higher betweenness centrality in these regions. These findings are in line with previous research that found that structural networks are altered in patients with CAA.[44]

Importantly, these changes in DTI measures were not yet visible in the presymptomatic phase of the diseases. Interestingly, a previous study has shown that in presymptomatic mutation carriers, the volume of white matter hyperintensities on fluid-attenuated inversion recovery imaging is slightly higher than in control participants.[45] This discrepancy likely is not caused by lower sensitivity of dMRI compared with white matter hyperintensity volume but rather by differences in approach. Because we used multiple approaches to analyzing the dMRI data, the statistical power was reduced by multiple comparison corrections. Still, the absence of significant differences between controls and presymptomatic carriers may be explained by the finding that white matter is still largely unaffected until a later stage of the disease. In patients with CAA, brain network connectivity in patients worsened measurably over 1.3-year follow-up.[13] This result is in line with our finding that the decline in global diffusion measures manifests mostly at a later age. This may suggest that the high sensitivity of dMRI in symptomatic carriers may not extrapolate to earlier, presymptomatic carriers or early cases of CAA.

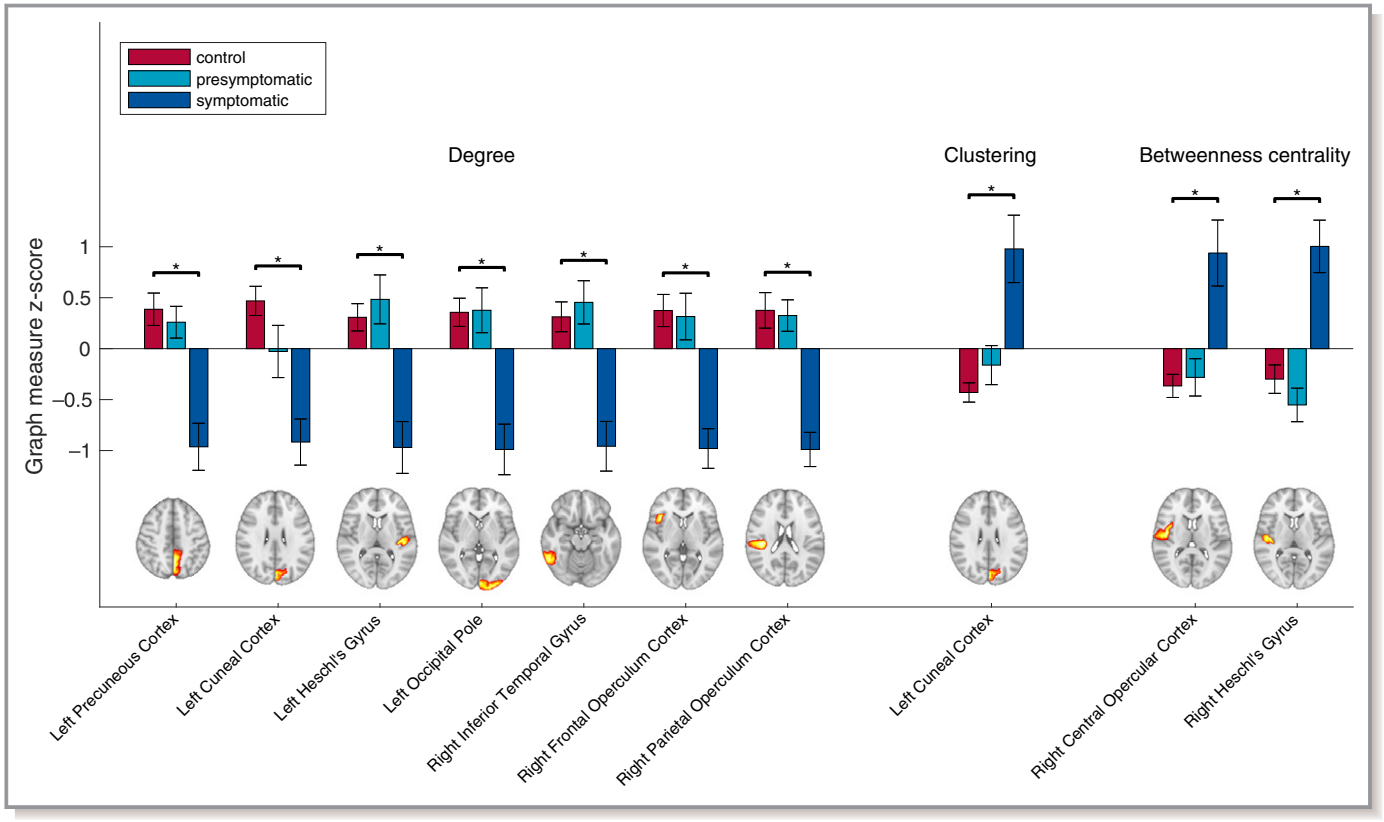

Figure 4. Significant structural connectomics measures averaged per group and with *z* scores for visualization. Means adjusted for age, sex, and proportional cerebrospinal fluid. **P*<0.05 (Familywise error corrected for regions, graph measures, and contrasts).

An important limitation of the present study is sample size. It is possible that the small sample size did not provide enough power to detect significant differences between presymptomatic carriers and controls. The rareness of the point mutation in the APP gene causing HCHWA-D makes it challenging to collect larger samples. Still, follow-up studies in a larger cohort of presymptomatic mutation carriers are needed to confirm that differences in dMRI-related connectivity are late markers for CAA. Another limitation is the limited number of diffusion directions and the relatively low b-value of 1000 s/mm^2 in the DWI protocol. A higher number of diffusion directions and a b-value of ≈3000 s/mm^2 would result in more accurate estimation of the fiber orientation distribution and more accurate construction of the structural connectomics, which may provide more power to detect group differences.

Sources of Funding

This study was supported by Vici grant 016.130.677 of the Netherlands Organization for Scientific Research. This study was supported by US National Institutes of Health grant R01NS070834.

Disclosures

None.

References

1. Vinters HV. Cerebral amyloid angiopathy. A critical review. *Stroke*. 1987;18:311–324.
2. Greenberg SM. Cerebral amyloid angiopathy: prospects for clinical diagnosis and treatment. *Neurology*. 1998;51:690–694.
3. Charidimou A, Gang Q, Werring DJ. Sporadic cerebral amyloid angiopathy revisited: recent insights into pathophysiology and clinical spectrum. *J Neurol Neurosurg Psychiatry*. 2012;83:124–137.
4. Alonzo NC, Hyman BT, Rebeck GW, Greenberg SM. Progression of cerebral amyloid angiopathy: accumulation of amyloid-beta40 in affected vessels. *J Neuropathol Exp Neurol*. 1998;57:353–359.
5. Greenberg SM. Cerebral amyloid angiopathy and vessel dysfunction. *Cerebrovasc Dis*. 2002;13:42–47.
6. Biffi A, Greenberg SM. Cerebral amyloid angiopathy: a systematic review. *J Clin Neurol*. 2011;7:1–9.
7. Reijmer YD, Van Veluw SJ, Greenberg SM. Ischemic brain injury in cerebral amyloid angiopathy. *J Cereb Blood Flow Metab*. 2016;36:40–54.
8. Wardlaw JM, Makin SJ, Valdés Hernández MC, Armitage PA, Heye AK, Chappell FM, Muñoz-Maniega S, Sakka E, Shuler K, Dennis MS, Thrippleton MJ. Blood-brain barrier failure as a core mechanism in cerebral small vessel disease and dementia: evidence from a cohort study. *Alzheimers Dement*. 2017;13:634–643.
9. Hartz AMS, Bauer B, Soldner ELB, Wolf A, Boy S, Backhaus R, Mihaljevic I, Bogdahn U, Klünemann HH, Schuierer G, Schlachetzki F. Amyloid-β contributes to blood-brain barrier leakage in transgenic human amyloid precursor protein mice and in humans with cerebral amyloid angiopathy. *Stroke*. 2012;43:514–523.
10. Charidimou A, Meegahage R, Fox Z, Peeters A, Vandermeeren Y, Laloux P, Baron J, Jäger HR, Werring DJ. Enlarged perivascular spaces as a marker of underlying arteriopathy in intracerebral haemorrhage: a multicentre MRI cohort study. *J Neurol Neurosurg Psychiatry*. 2013;84:624–629.
11. Charidimou A, Jaunmuktane Z, Baron J, Jäger R. White matter perivascular spaces. *Neurology*. 2014;82:57–62.
12. Martinez-Ramirez S, Pontes-Neto OM, Dumas AP, Auriel E, Halpin A, Quimby M, Gurol ME, Greenberg SM, Viswanathan A. Topography of dilated

perivascular spaces in subjects from a memory clinic cohort. *Neurology*. 2013;80:1551–1556.

13. Reijmer YD, Fotiadis P, Riley GA, Xiong L, Charidimou A, Boulouis G, Ayres AM, Schwab K, Rosand J, Gurol ME, Viswanathan A, Greenberg SM. Progression of brain network alterations in cerebral amyloid angiopathy. *Stroke*. 2016;47:2470–2475.
14. Reijmer YD, Fotiadis P, Charidimou A, Van Veluw SJ, Xiong L, Riley GA, Martinez-ramirez S, Schwab K, Viswanathan A, Gurol ME, Greenberg SM. Relationship between white matter connectivity loss and cortical thinning in cerebral amyloid angiopathy. *Hum Brain Mapp*. 2017;38:3723–3731.
15. Salat DH, Smith EE, Tuch DS, Benner T, Pappu V, Schwab KM, Gurol ME, Rosas HD, Rosand J, Greenberg SM. White matter alterations in cerebral amyloid angiopathy measured by diffusion tensor imaging. *Stroke*. 2006;37:1759–1764.
16. Levy E, Carman MD, Fernandezmadrid IJ, Power MD, Lieberburg I, Vanduinen SG, Bots G, Luyendijk W, Frangione B. Mutation of the Alzheimers-disease amyloid gene in hereditary cerebral-hemorrhage, Dutch type. *Science (80-)*. 1990;248:1124–1126.
17. Bornebroek M, Haan J, Maat-Schieman ML, Van Duinen SG, Roos RA. Hereditary cerebral hemorrhage with amyloidosis-Dutch type (HCHWA-D): I—A review of clinical, radiologic and genetic aspects. *Brain Pathol*. 1996;6:111–114.
18. Maat-Schieman ML, van Duinen SG, Bornebroek M, Haan J, Roos RA. Hereditary cerebral hemorrhage with amyloidosis-Dutch type (HCHWA-D): II—A review of histopathological aspects. *Brain Pathol*. 1996;6:115–120.
19. Zhang-Nunes SX, Maat-Schieman MLC, Van Duinen SG, Roos RAC, Frosch MP. The cerebral β-amyloid angiopathies : hereditary and sporadic. *Brain Pathol*. 2006;16:30–39.
20. Grieve SM, Williams LM, Paul RH, Clark CR, Gordon E. Cognitive aging, executive function, and fractional anisotropy: a diffusion tensor MR imaging study. *AJNR Am J Neuroradiol*. 2007;28:226–235.
21. Smith SM, Jenkinson M, Woolrich MW, Beckmann CF, Behrens TEJ, Johansen-Berg H, Bannister PR, De Luca M, Drobnjak I, Flitney DE, Niazy RK, Saunders J, Vickers J, Zhang Y, De Stefano N, Brady JM, Matthews PM. Advances in functional and structural MR image analysis and implementation as FSL. *Neuroimage*. 2004;23:S208–S219.
22. Jenkinson M, Beckmann CF, Behrens TEJ, Woolrich MW, Smith SM. Fsl. *Neuroimage*. 2012;62:782–790.
23. Smith SM, Jenkinson M, Johansen-Berg H, Rueckert D, Nichols TE, Mackay CE, Watkins KE, Ciccarelli O, Cader MZ, Matthews PM, Behrens TEJ. Tract-based spatial statistics: voxelwise analysis of multi-subject diffusion data. *Neuroimage*. 2006;31:1487–1505.
24. Baykara E, Gesierich B, Adam R, Tuladhar AM, Biesbroek JM, Koek HL, Ropele S, Jouvent E, Chabriat H, Ertl-Wagner B, Ewers M, Schmidt R, de Leeuw FE, Biessels GJ, Dichgans M, Duering M. A novel imaging marker for small vessel disease based on skeletonization of white matter tracts and diffusion histograms. *Ann Neurol*. 2016;80:581–592.
25. Beckmann CF. Modelling with independent components. *Neuroimage*. 2012;62:891–901.
26. Desikan RS, Ségonne F, Fischl B, Quinn BT, Dickerson BC, Blacker D, Buckner RL, Dale AM, Maguire RP, Hyman BT, Albert MS, Killiany RJ. An automated labeling system for subdividing the human cerebral cortex on MRI scans into gyral based regions of interest. *Neuroimage*. 2006;31:968–980.
27. Zhan L, Zhou J, Wang Y, Jin Y, Jahanshad N, Prasad G, Nir TM, Leonardo CD, Ye J, Thompson PM. Comparison of 9 tractography algorithms for detecting abnormal structural brain networks in Alzheimer's disease. *Front Aging Neurosci*. 2015;7:1–19.
28. Smith RE, Tournier JD, Calamante F, Connelly A. Anatomically-constrained tractography: improved diffusion MRI streamlines tractography through effective use of anatomical information. *Neuroimage*. 2012;62:1924–1938.
29. Smith RE, Tournier JD, Calamante F, Connelly A. SIFT: spherical-deconvolution informed filtering of tractograms. *Neuroimage*. 2013;67:298–312.
30. Yeh CH, Smith RE, Liang X, Calamante F, Connelly A. Correction for diffusion MRI fibre tracking biases: the consequences for structural connectomic metrics. *Neuroimage*. 2016;142:150–162.
31. Tournier JD, Calamante F, Connelly A. MRtrix: diffusion tractography in crossing fiber regions. *Int J Imaging Syst Technol*. 2012;22:53–66.
32. Zhang Y, Brady M, Smith S. Segmentation of brain MR images through a hidden Markov random field model and the expectation-maximization algorithm. *IEEE Trans Med Imaging*. 2001;20:45–57.
33. Patenaude B, Smith SM, Kennedy DN, Jenkinson M. A Bayesian model of shape and appearance for subcortical brain segmentation. *Neuroimage*. 2011;56:907–922.
34. Tax CMW, Jeurissen B, Vos SB, Viergever MA, Leemans A. Recursive calibration of the fiber response function for spherical deconvolution of diffusion MRI data. *Neuroimage*. 2014;86:67–80.
35. Tournier J-D, Calamante F, Connelly A. Improved probabilistic streamlines tractography by 2nd order integration over fibre orientation distributions. *Proceedings of the International Society for Magnetic Resonance in Medicine*. 2010;88:2010.
36. Smith RE, Tournier JD, Calamante F, Connelly A. The effects of SIFT on the reproducibility and biological accuracy of the structural connectome. *Neuroimage*. 2015;104:253–265.
37. Rubinov M, Sporns O. Complex network measures of brain connectivity: uses and interpretations. *Neuroimage*. 2010;52:1059–1069.
38. Smith SM, Nichols TE. Threshold-free cluster enhancement: addressing problems of smoothing, threshold dependence and localisation in cluster inference. *Neuroimage*. 2009;44:83–98.
39. Winkler AM, Ridgway GR, Webster MA, Smith SM, Nichols TE. Permutation inference for the general linear model. *Neuroimage*. 2014;92:381–397.
40. Winkler AM, Ridgway GR, Douaud G, Nichols TE, Smith SM. Faster permutation inference in brain imaging. *Neuroimage*. 2016;141:502–516.
41. Duan J-H, Wang H-Q, Xu J, Lin X, Chen S-Q, Kang Z, Yao Z-B. White matter damage of patients with Alzheimer's disease correlated with the decreased cognitive function. *Surg Radiol Anat*. 2006;28:150–156.
42. Zhu Y-C, Chabriat H, Godin O, Dufouil C, Rosand J, Greenberg SM, Smith EE, Tzourio C, Viswanathan A. Distribution of white matter hyperintensity in cerebral hemorrhage and healthy aging. *J Neurol*. 2012;259:530–536.
43. Bassett DS, Bullmore E, Verchinski BA, Mattay VS, Weinberger DR, Meyer-Lindenberg A. Hierarchical organization of human cortical networks in health and schizophrenia. *J Neurosci*. 2008;28:9239–9248.
44. Reijmer YD, Fotiadis P, Martinez-Ramirez S, Salat DH, Schultz A, Shoamanesh A, Ayres AM, Vashkevich A, Rosas D, Schwab K, Leemans A, Biessels GJ, Rosand J, Johnson KA, Viswanathan A, Gurol ME, Greenberg SM. Structural network alterations and neurological dysfunction in cerebral amyloid angiopathy. *Brain*. 2015;138:179–188.
45. Van Rooden S, Van Opstal AM, Labadie G, Terwindt GM, Wermer MJH, Webb AG, Middelkoop HAM, Greenberg SM, Van Der Grond J, Van Buchem MA. Early magnetic resonance imaging and cognitive markers of hereditary cerebral amyloid angiopathy. *Stroke*. 2016;47:3041–3044.